Use of site symmetry in supercell model of defective crystals:polarons in CeO_2

R. A. Evarestov[1], D. Gryaznov[2], M. Arrigoni[3], E. A. Kotomin[2,3], A. Chesnokov[2], J. Maier[3]

[1]St. Petersburg University, Universitetsky Prosp. 26, 198504, St. Petersburg, Russia

[2]Institute for Solid State Physics, University of Latvia, Kengaraga 8, LV-1063 Riga, Latvia

[3]Max Planck Institute for Solid State Research, Heisenbergstr. 1, D-70569 Stuttgart, Germany

Keywords: CeO_2, site symmetry, oxygen vacancy, polaron, first principles calculations

ABSTRACT: It was not noticed so far, that the commonly used supercell model for defective crystals imposes certain site symmetry restrictions on atoms therein. In this paper, a novel approach is suggested: while choosing the supercell size of defective crystals, instead of a trial-and-error approach for the defect position, it is necessary to analyze first the site symmetry of the split Wyckoff positions of the perfect crystal atoms (which will be substituted or removed in defective crystals) and perform defect calculations for different possible site symmetries, to find the energetically most favorable defect configuration. Using CeO_2, as an example, it is demonstrated that use of site symmetry of the removed oxygen atoms in supercells with vacancies allows obtaining all possible atomic and magnetic polaron configurations, and predict which vacancy positions correspond to the lowest formation energies associated with small polarons. We give a simple symmetry based explanation on the existence of controversies in the

literature on the nature of oxygen vacancies in CeO_2. In particular, the experimentally observed small polaron formation could arise for oxygen vacancies with the lowest C_s site symmetry, existing in 3 x 3 x 3 and larger supercells. The results of first principles calculations with linear combination of atomic orbitals and hybrid exchange-correlation functionals are compared with those from previous studies, obtained using a standard DFT+U approach.

1. INTRODUCTION

Cerium oxide, CeO_2 (ceria) continues to attract great interest due to its high ionic conductivity and use as electrolyte in solid oxide fuel cells (being acceptor doped), catalysis, resistive switching and other technological applications.[1,2] Pure ceria shows small polaron conductivity.[3] The electrons form polarons corresponding to distinct Ce^{3+} ions, compensated by positively charged oxygen vacancies. Thus, it is not surprising that polaron properties of ceria were subject of numerous experimental and theoretical studies.[4-8] Nowadays it is well established that the calculations on CeO_2 should take into account strong electron correlation effects. Most of the previous studies used the GGA+U approach, with several rare exceptions.[5.8] In the DFT+U approach, formation of small polarons depends critically on the choice (or even fitting) of the Hubbard-U parameter.[5] An alternative, more advanced approach is to use the hybrid exchange-correlation functionals, as done in this paper.

Another common and poorly discussed problem is the choice of the supercell size in defect modelling. Relatively small supercells are commonly used to reduce computational efforts, since all atoms of same type (e.g. oxygens) were considered to be equivalent. It is also a common to reduce system symmetry during the calculation in order to force electron localization on Ce^{3+} ions thus forming small polaron. We demonstrate, however, that the oxygens – even in non-

defective supercells – are not equivalent by symmetry. As a result, oxygen atoms in the supercell different by site symmetry have quite different vacancy formation energies and what is more, only some of them could be related to small polarons without imposing an artificial symmetry reduction (see our discuss below in Sec. 4). In other words, the proper size of supercell should be chosen, as to guarantee the presence of oxygen vacancies (in Kröger-Vink notations[9]: $V_O^{\bullet\bullet}$) with low site symmetry allowing for formation of two reduced Ce^{3+} ions nearby. We analyze the site symmetry of oxygen atoms in different CeO_2 supercells and show that for polaronic defects to exist in CeO_2 the oxygen site symmetry should be C_s or C_{2v} existing only in the 3 x 3 x 3 supercells (containing 81 atoms, equivalent to a defect concentration of ~2%) and larger supercells.

2. SITE SYMMETRY APPROACH TO POINT DEFECT CALCULATIONS IN SUPERCELL MODEL

The crystalline solid with a point defect (defective crystal) constitutes formally an aperiodic system. In the supercell model (SCM) of a defective crystal an artificial defect periodicity is introduced which allows one to use the same calculation schemes and computer codes both for the host (perfect) and defective crystals.

Despite the common use of the SCM nowadays, its symmetry analysis is very rare[10-12], and even these publications contain no discussion on the possibility of different choices of the site symmetry of the substituted or removed atoms. Such a possibility was considered only recently[13] for determining the magnetic symmetry groups of the wurtzite-type crystals doped with magnetic atoms periodically distributed at cation sites. Starting from a highly symmetrical wurtzite structure type and reducing the space-group symmetry, less symmetric structure types were

obtained and the splitting schemes of the occupied Wyckoff positions were taken into account. It was shown that the type of magnetic ordering depends not only on the symmetry group of the magnetic semiconductor but also on the site symmetry of impurities. Within this procedure, all possible magnetic groups and corresponding magnetic structures for different distributions of the magnetic impurities over the cation sublattice sites of the host lattice were obtained.[13]

Let us assume that in the SCM periodically repeated point defects be placed in the positions with the site symmetry S_d corresponding to the substituted atom or vacancy. In the case when the perfect crystal has the symmetry of space group $G = T_a F$, the SCM of the defective crystal is described by space group $G_d = T_A F_d$. Here G_d, T_A and F_d are subgroups of G, T_a and F, respectively.

The supercell translation group T_A consists of translations t_A of the supercell and is defined by the transformation matrix chosen for the supercell generation[9]. The basic supercell translation vectors A_j of the new direct lattice L_2 are defined by a linear transformation of the basic translations $\mathbf{a}_i$ of the initial direct lattice L_1:

$$\mathbf{A}_j(L_2) = \sum_i l_{ji}\, \mathbf{a}_i\,(L_1) \qquad (1)$$

where l_{ji} are integer elements of the matrix l defining the transition from the lattice of type L_1 to the lattice of type L_2. By a definition, for the symmetrical transformation l the point symmetry of lattices L_2 and L_1 is the same. The symmetrical transformation matrices l in Eq. (1) for all 14 types of Bravais lattices are given in Ref. 10. The diagonal form of matrix L is a particular case of the symmetrical transformation (1) and is traditionally applied in SCM of defective crystals.

The point group F_d of the defective crystal is defined by the site symmetry group S_d. Unfortunately, the analysis of possible S_d choice is absent in papers applying SCM to defective

crystals. Traditionally S_d is chosen as the point symmetry group of the substituted or removed atom in the host crystal primitive unit cell.

Let us consider the particular case of a CeO_2 crystal with fluorite structure (space group Fm-3m, face-centered cubic lattice). Its primitive unit cell consists of three atoms, whereas a conventional cell has 12 atoms (Figs.1 and 2). Ce atom occupies Wyckoff position at (000) with site symmetry S48=O_h (m-3m). We use the abbreviation SN for the site symmetry group of N point operations. Two oxygen atoms occupy Wyckoff position 2c (0.25, 0.25, 0.25; -0.25, -0.25, -0,25) so that site symmetry group of oxygen atom is S24=T_d . Thus, the primitive unit cell of ceria contains two orbits occupied by atoms transforming into each other under point symmetry operations: S48 with site symmetry O_h (Ce orbit) and S24 with site symmetry T_d (oxygen orbit).

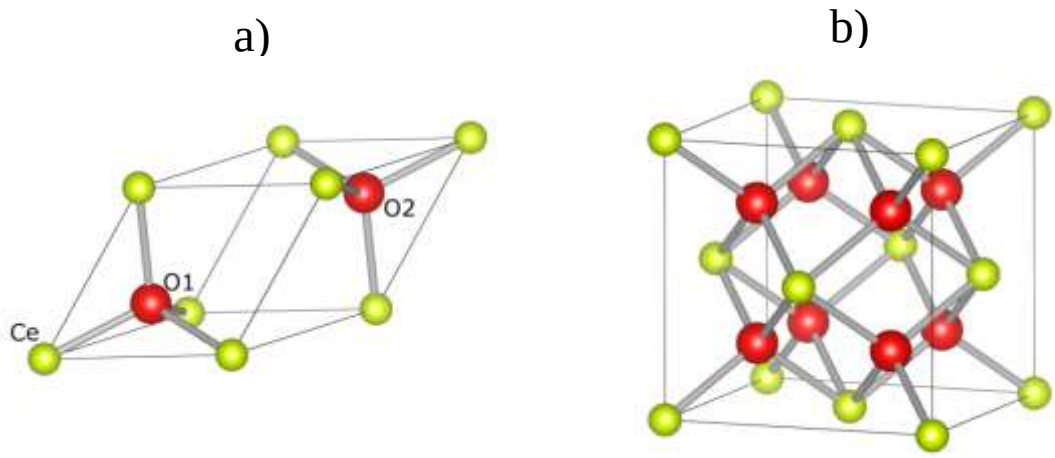

Figure 1. a) Primitive CeO_2 unit cell, consisting of 3 atoms and two orbits: S48 (Ce-orbit), S24 (O-orbit); b) Conventional CeO_2 unit cell, consisting of 12 atoms and two orbits. Ce and O atoms are marked in green-yellow and red colors, respectively.

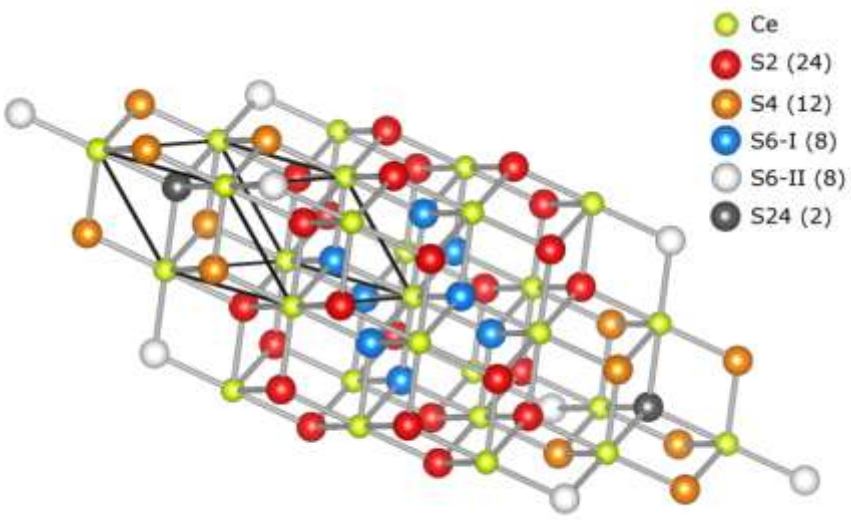

Figure 2. L27 supercell (see table 1 for details): distribution of oxygen atoms over 5 orbits (shown in different colors) S2 (red), S4 (dark yellow), S6-I (blue), S6-II (bright grey), S24 (dark grey), and the rest Ce atoms (green-yellow).

Let the 3 x 3 x 3 supercell be chosen for the neutral oxygen vacancy modeling, i.e. matrix (1) in Eq. (1) chosen to be diagonal and retaining the cubic face-centered symmetry of the host lattice. In the traditional SCM, the oxygen atom is removed from the atomic oxygen position S24 (with site symmetry T_d). In such a case, it is ignored that in the chosen supercell of 81 atoms (27 primitive cells) 54 oxygen atoms are split in 5 orbits, shown in Fig 2. The use of the program WYCKSPLIT[14] allows us determination of the space group Wyckoff positions splitting in the sub-groups, defined by the supercell choice. The application of this program for space group (SG) of a host crystal No 225 and diagonal lattice transformation matrix 3x3x3 shows that oxygen orbit S24 of two atoms is only one of these 5 split orbits: S4 (12 atoms), two S6 orbits (2x8 atoms) and S2 orbit (24 atoms). The corresponding site symmetry point groups for low symmetry orbits are C_s(S2), C_{2v} (S4) and C_{3v} (S6), respectively. The distribution of oxygen atoms over orbits depends on the supercell choice, see Table 1.

Table 1. Oxygen site symmetry in different size supercells, LX(Y): X is the number of unit cells, Y the number of atoms in the supercell, SX-number of point symmetry operations in orbit supercell.

L1(3)	L8 (24)	L27 (81)	L64 (192)	L32 (96, 64)
T_d(S24)	2 x C_{3v}(S6)	C_s(S2); 2 x C_{3v}(S6)	4 x C_s(S2); 4 x C_{3v}(S6)	2 x C_s(S2);2 x C_{3v}(S6)
		C_{2v}(S4); T_d(S24)		

The modeling of the oxygen vacancy could be performed using not only the high symmetry position S24, but also removing oxygen atoms from orbits S2, S4 and S6. The defect concentration in all these cases remains the same (1/54=1.8%), as the distance between the vacancies in the neighboring supercells is the same and defined by the supercell translation vector length.

We show in the present paper that the choice of the $V_O^{\bullet\bullet}$ position in the oxygen orbits with different point site symmetry is important, as it defines not only the calculated oxygen vacancy formation energy but also the local lattice distortion and the character of the electron density localization in the defective crystal.

3. COMPUTATIONAL DETAILS AND BASIC BULK PROPETIES OF CeO_2

In the present calculations, a basis set (BS) of the linear combination of atomic orbitals (LCAO), and Perdew-Burke-Ernzerhof[15] hybrid exchange-correlation functional PBE0 (hereafter, functional) were used, as implemented in the CRYSTAL14 computer code.[16] It is well established that the hybrid DFT functionals or the alternative DFT+U approach are necessary to avoid the problem of metallic behavior of CeO_2 as obtained in the LDA, GGA calculations. The LCAO approach together with the hybrid PBE0 and/or HSE06 functionals allow us performing highly accurate first-principles calculations, which is in particular important for the studies of

electron localization effects in CeO_2. The hybrid PBE0 and HSE06 functionals suppose 25% of the exact non-local exchange (α=0.25 is the mixing parameter). However, the HSE06 functional belongs to the family of range-separated hybrid functionals in which the amount of exact exchange depends on the distance between the electrons.[17] Thus, the HSE06 functional supposes the empirical splitting parameter of 0.11 $Bohr^{-1}$ to split the Coulomb operator into short and long range components. It has been shown by us in Ref. 18 and other authors[19] that PBE0 correctly reproduces the basic properties and defect behavior in different oxides. Besides, it was shown[20] that there exists a simple relation for some oxides between the α parameter and the high frequency dielectric constant (ε^{∞}). Indeed, the $\alpha \sim 1/\varepsilon^{\infty}$ relation is valid for CeO_2 (table 2) as well. We laid emphasis on the analysis of calculated electronic density of states (DOS), atomic (Mulliken) charges, the z-projection of the magnetic moments (hereafter, magnetic moments) of Ce in defective CeO_2, the Ce-O bond lengths as well as the energetics of several types of oxygen vacancies.

The quasi-relativistic BS for Ce was taken from the LCAO calculations.[21] It included the effective core potential, to replace 28 inner electrons. The all-electron 8-411G BS of O atoms[22] was already successfully used by us in previous studies.[18,23] It should be emphasized that we optimized the BS for CeO_2 using the Powell's conjugate-directions minimization method without calculations on the total energy derivatives, as implemented in the code OPTBAS.[24] The BS optimization was performed using the hybrid HSE06 functional, and we compare the basic bulk properties of CeO_2 for both hybrid PBE0 and HSE06 functionals (see below).

Table 2. Basic bulk and mechanical properties of defect-free CeO_2

Property	Expt.	PBE0 (HSE06)	GGA+U	LDA

		present study		
Conventional cell parameter (Å)	5.406[a] 5.411[b]	5.393 (5.396)	5.494[f] 5.429[g] 5.426[h]	5.330[i], 5.366[j]
Band gap (O2p-Ce4f) (eV)	3[c]	4.32 (3.64)	2.35[f]	-
Band gap (O2p-Ce5d) (eV)	6.0 – 8.0[c]	8.24 (7.57)	5.31[f]	-
Bulk Modulus (GPa)	204[d]-220[b]	219.0 (218.1)	181[f] 207[h]	218[i], 210.1[j]
C11 (GPa)	403[d]	426.0 (423.4)	391[h]	399.5[i], 386[j]
C12 (GPa)	105[d]	115.5 (115.5)	129[h]	127.5[i], 124[j]
C44 (GPa)	60[d]	65.4 (64.7)	57[h]	63.5[i], 73[j]
Cohesive Energy (eV)	-21[e]	-19 (-19)	-	-

[a]Ref. 31. [b]Ref. 32. [c]Ref. 33. [d]Ref. 34. [e]Ref. 35 and references therein. [f]Ref. 4. [g]Ref.36. [h]Ref. 37. [i]Ref. 38. [j]Ref. 39.

The standard Monkhorst-Pack scheme[25] for 2 x 2 x 2 and 6 x 6 x 6 *k*-point mesh in the Brillouin zone was applied for the 3x3x3 supercell and primitive unit cell of CeO_2, respectively. Tolerance factors of 8, 8, 8, 8, 20 for the Coulomb and exchange integrals were used.[16] Furthermore, the SCF convergence threshold on the total electron energy is set to 10^{-9} a.u. while the threshold on the energy change between the full structure optimization steps is set to 10^{-8} a.u. All defect calculations in the CRYSTAL code were spin polarized. We used the frozen phonon (direct method)[26-27] in the calculations of vibrational frequencies. The high-frequency dielectric constant was estimated using the coupled perturbed HF/Kohn-Sham method[28-30] as implemented in the CRYSTAL code. The threshold on the energy change for this property was set at 10^{-4} a.u.

It allows us to determine with high accuracy the longitudinal optical (LO) phonon frequency and static dielectric constants in pure CeO_2.

Table 2 summarizes the basic bulk properties of CeO_2 calculated using different functionals. Our calculated lattice constant using both the HSE06 and PBE0 hybrid functionals is in good agreement with not only experiments but also previous hybrid functional calculations: e.g. 5.38 Å for B1WC.[21] The lattice constants in the two DFT+U calculations differ slightly between each other (despite the same value of U = 5.0 eV) and larger than experimental value. It could explain why the bulk modulus from the DFT+U calculation[4] is smaller than our calculated and experimental values. On the other hand, as expected, the standard LDA functional significantly underestimates the lattice constant (surprisingly, its bulk modulus value is still in a line with our calculated value). The PBE0/HSE calculated elastic constants are also in good agreement with the experimental values and previous calculations.

In table 3 the calculated phonon frequencies and dielectric constants are given. The PBE0/HSE06 calculated T_{1u} and T_{2g} vibrational modes of the present study are very consistent with the measured ones. As seen in table 3, the hybrid functionals should be used to properly calculate the phonon frequencies. Nevertheless, in contrast to the T_{1u} mode, our calculated T_{2g} mode is better reproduced in comparison with the previous HSE calculations by Wang et al.[42]

In CeO_2 the valence band top is mainly of O *2p* character, and the band gap between the O *2p* band and unoccupied Ce *5d* states (O2p-Ce5d) is estimated as 8.2 eV in our PBE0 calculations. In table 2 we also give the energy distance between the O *2p* band and an unoccupied (polaronic) Ce-*4f* band (O2p-Ce4f) lying between these two bands gaps.[5] Both energies are slightly overestimated/underestimated with the PBE0/DFT+U functionals but better reproduced with the HSE06 functional. The GGA+U underestimate these energies. Due to considerable

computational difficulties related to the HSE06 functional in calculations of supercells in the CRYSTAL code, we performed calculations for defective CeO_2 with the 3 x 3 x 3 supercell using the PBE0 functional only.

Table 3. Phonon properties of defect-free CeO_2

Property	Expt.	PBE0 (HSE06) present study	HSE[d]	LDA[e]
Static dielectric constant, ionic part ε^0	17[a]	17.4 (17.5)	-	16.7
High frequency dielectric constant ε^∞	5.31[b], 6[a]	5.28	5.7	6.2
T.O. T1u vibration (cm^{-1})	272[c]	295 (293)	264	301
T2g vibration (cm^{-1})	465[c]	470 (468)	451	-
L.O. (cm^{-1})	595[c]	612 (607)	573	579

[a]Ref. 40. [b]Ref. 38. [c]Ref. 41. [d]Ref. 42. [e]Ref. 39

The oxygen vacancies in supercells were modeled by a removal of oxygen atoms in positions with different site symmetry. The formation energy of a $V_O^{\bullet\bullet}$ in a totally uncharged supercell was calculated according to relation

$$E_F = E_{tot}^{V_O^{\bullet\bullet}} - E_{tot}^{p} + \mu_o \quad , \qquad (2)$$

where superscripts p and $V_O^{\bullet\bullet}$ stand for the perfect and defective (one $V_O^{\bullet\bullet}$ per supercell) crystals, $E_{tot}^{V_O^{\bullet\bullet}}$ and E_{tot}^{p} are total electron energy, respectively, μ_O represents the chemical potential of a

free oxygen atom calculated as a half of the total electron energy of a gas-phase O_2 molecule. Notice that the LCAO approach with the PBE0 functional – unlike the plane wave calculations--reproduces very well the properties of the O_2 molecule.[18] The electrons of a missing oxygen atom are delocalized from vacancy over nearest Ce ions forming small and large polarons discussed below.

4. POLARON CALCULATIONS

The calculations of $V_O^{\bullet\bullet}$ were performed using the supercell L27, obtained by three times increasing all primitive fcc (face centered cubic) lattice translation vectors and consisting of 54 oxygen atoms, split into 5 orbits (S2, S4, S6-I, S6-II and S24; see Section 2 and Figure 2 for explanation). Interestingly, in ionic MgO vacancy formations is associated with the *F*-color centers where the two electrons are well localized at the vacancy site. In contrast, the semi-covalent CeO_2 is characterized by the Ce 4f-type conduction sub-band filled with electrons in the presence of $V_O^{\bullet\bullet}$. For the present analysis of the magnetic configurations only those 4 Ce atoms are chosen which were nearest to the removed oxygen atom in the perfect crystal. The two electrons from a missing O ion turn out to be localized either on the two nearest Ce ions, or delocalized over three to four nearest Ce ions (called, hereafter, small and large polarons, respectively). In the following we present the results of calculations for vacancies with different site symmetries and accordingly different degrees of the electron localization.

In table 4 detailed information is collected on the number of displaced Ce atoms (N) with localized electrons, the magnetic moments (μ's) on these Ce atoms, the distance between the Ce atom with localized electron and the closest O atom, the changes of distances between the Ce

atoms caused by the $V_O^{\bullet\bullet}$ formation (the positive sign means outward displacement), and the vacancy formation energy E_F (Eq. 2) with respect to the lowest energy state with spin projection $S_z = 0$ state for the site symmetry point group C_s(S2). The corresponding formation energy E_F of $V_O^{\bullet\bullet}$ equals 4.10 eV. Notice that the value of S_z in table 4 is defined by a starting magnetic configuration whereas the calculated magnetic configuration is seen from μ's on Ce atoms. The excellent review paper[8] on vacancy formation energies in CeO_2 with the standard DFT and DFT+U functionals for different U-values demonstrated a very broad range of results. Emphasis was laid on the analysis of the electronic structure changes but we suggest that the discussion of a role of site symmetry is still lacking but needed for a better understanding of calculation results.

We aim to address the site symmetry effects on the properties of CeO_2 with vacancies. In order to better explain the possible magnetic configurations appearing in this case, we use the following notations in table 4: (Ce1, Ce2)(Ce3)(Ce4) for S2, (Ce1,Ce2)(Ce3, Ce4) for S4, (Ce1)(C2, Ce3, Ce4) for S6, (Ce1, Ce2, Ce3, Ce4) for S24 where only the Ce atoms in the paranthesis are equivalent by symmetry (i.e., belonging to the same orbit). Knowing the Ce atoms distribution over orbits with the different point symmetry, it is possible to indicate the Ce atoms with spins, denoted by '+', and those without the spin denoted by '-' in table 4, for starting magnetic configurations. Thus, we present the results for the magnetic configuration which differ by the value of S_z for each vacancy site. We demonstrate that the number of S_z-values depends exclusively on the $V_O^{\bullet\bullet}$ site symmetry. So, the calculation of $V_O^{\bullet\bullet}$ for the lowest symmetry point group C_s(S2) is characterized by the largest number of magnetic configurations and the S_z-values of 0, ½, 1, 3/2, and 2. In contrast, the calculation of $V_O^{\bullet\bullet}$ for the highest symmetry point group T_d (S24) suggests one magnetic configuration only and, consequently, the

S_z value of 2 (table 4). Notice that the Ce atoms of the same orbit should have the same value of S_z: 0, 1/2 or -1/2. In other words, the $V_O^{\bullet\bullet}$ site symmetry dictates how the spins distribute over the four Ce atoms in the supercell. The S2 orbit has two equivalent and two non-equivalent Ce atoms whereas the S24 orbit has four equivalent Ce atoms.

Table 4. All magnetic configurations allowed by the $V_O^{\bullet\bullet}$ point symmetry in the calculations of L27 supercell. In the first column we give the site symmetry SN (N = 2, 4, 6, 24) of removed oxygen atom and the corresponding distribution of four Ce atoms (nearest to oxygen atom in perfect crystal) over the point symmetry orbits defined by oxygen (atoms belonging to the same orbit are given in brackets). The Ce atoms of the same orbit can have the same spin projection (0, 1/2 or-1/2). In the second column the total Ce atoms spin projection S_z is given for each magnetic configuration considered. S_z is defined by a starting magnetic configuration whereas the calculated magnetic configuration is seen from μ's. The Ce atoms with spin are denoted by '+' and those without the spin are denoted by '-'. N is the number of displaced Ce atoms (column 3) with the magnetic moment μ/μ_B (column 4) ; d(Ce-O) is the bond length between the displeced Ce atom with localized electron and the closest O atom (column 5), Δd(Ce-Ce) in column 6 gives the changes in the distance between the Ce atoms after relaxation (the positive sign means move away from $V_O^{\bullet\bullet}$; see the text for explanations), ΔE_F (column 7) represents the vacancy formation energy (Eq. 2) difference with respect to the $S_z = 0$ state of point symmetry C_s(S2) (as being the lowest energy state with the formation energy of 4.10 eV) for each magnetic configuration. The last column gives the supercell volume for the structure optimized supercell with $V_O^{\bullet\bullet}$.

Site Symmetry / Symmetry equivalence of Ce atoms	Spin projection (S_z)	N	μ/μ_B	d(Ce-O) / Å*	Δd(Ce-Ce) / Å**	ΔE_F / meV	Volume / Å^{3***}
Cs (S2) / (Ce1, Ce2)(Ce3)(Ce4)	0 (--)(+)(+)	2	0.96 -0.96	2 x 2.30	0.17 0.23 0.30	0	1068.07
	½ (++)(-)(+)	3	0.96 2 x -0.49	2.30 2 x 2.24	0.20 0.22 0.20	306	1067.47
	1 (-,-)(+)(+)	2	2 x 0.96	2 x 2.30	0.17 0.23 0.30	0.2	1068.06
	3/2 (+,+)(-)(+)	3	0.96 2 x 0.50	2.25 2.25 2.31	0.21 0.23 0.21	~338	1067.27
C2v (S4) / (Ce1, Ce2) (Ce3, Ce4)	0 (+,+)(+,+)	4	2 x +0.49 2 x -0.49	2 x 2.25	0.22 0.22 0.23	610	1066.56
	1 (-,-)(+,+)	2	2 x 0.96	2 x 2.30	0.17 0.23 0.30	0.2	1068.08
	2 (+,+)(+,+)	4	4 x 0.49	4 x 2.25	0.22 0.22 0.23	611	1066.50
C3v (S6) / (Ce1)(Ce2, Ce3, Ce4)	1 (+)(+,+,+,)	4	-0.95 3 x 0.35	2.30 3 x 2.23	0.21 0.24	432	1066.67
	3/2 (-)(+,+,+,)	3	3 x 0.65	3 x 2.27	0.22 0.26	396	1067.82
	2 (+)(+,+,+)	4	0.97 3 x 0.35	2.30 3 x 2.23	0.21 0.24	431	1066.82
Td (S24) / (Ce1, Ce2, Ce3, Ce4)	2 (+,+,+,+)	4	4 x 0.49	4 x 2.24	0.25	768	1066.71

*2.34 Å Ce-O distance in the perfect crystal

** 3.82 Å Ce-Ce distance in the perfect crystal

*** 1059.19 Å^3 the volume of perfect crystal

One of the most interesting cases here is due to $S_z = 0$ for S2 with the two non-equivalent Ce atoms accomodating an opposite spin alignment (we also call this case as anti-ferromagnetic,

AFM, and small polaron solution, for comparison with the literature data). The absolute values of the μ's of corresponding Ce atoms are 0.96 μ_B (table 4) meaning that the other two nearest Ce atoms have zero magnetic moments. From the calculation for S2 with $S_z = 0$ one could observe that the initial μ-values (~0.76 μ_B) on the two non-equivalent Ce atoms are increased up to 0.96 μ_B when the Ce atoms move towards $V_O^{\bullet\bullet}$ during the process of structure relaxation, in order to reach the total energy minimum. This is a typical behavior of the polarons. The energy difference between the $S_z = 0$ (AFM) and the $S_z = 1$ (ferromagnetic solution, denoted as FM and given by the same spin alignment of the two Ce atoms, and the μ-values of 0.96 μ_B) small polaron solutions is very small, ~0.2 meV. This fact is very much in accordance with the literature data.[7] So, these results confirm the existence of small radius polarons and their energetic preference in reduced CeO_2. However, the present site symmetry analysis shows that the small polaron solution with $S_z = 0$ is only possible for the site symmetry point group C_s(S2) and is not possible for other point groups (C_{2v}(S4), C_{3v}(S6) or T_d(S24)) without imposing an artificical symmetry reduction, probably used e.g. in Ref. 7. Moreover, we should emphasize that the S2 orbit appears only in the L27 and larger supercells (see also table 1). It is worth mentioning that the migration energy of small polarons could be estimated as the difference in the total energies of small and large polarons, mimicking the delocalized state (e.g., the case of $S_z = 1$ and 2 for S4 representing small and large polaron solutions, respectively). The estimated migration energy is ~0.6 eV (see table 4) being, thus, very close to the experimental value.[3]

Using the same notations, we obtain S_z = 0, 1, 2 and ½, 3/2, 1, 2 for the symmetry point groups C_{3v}(S4) and C_{2v}(S6), respectively. From the symmetry point of view, the two S6 orbits are not distinguishable. So, only one S6 orbit was considered in our calculations. Interestingly, the S6 orbit has one non-equivalent Ce atom and three equivalent Ce atoms (table 4). It gives rise

to $S_z = 3/2$ when the three equivalent Ce atoms have an equal value of $\mu \sim 0.65\ \mu_B$ but one non-equivalent Ce atom has the μ close to 0 (large polaron). We should emphasize that the values of $S_z = 2$ for S2 and ½ for S6 are missing in table 4 as these were not possible to calculate due to high computational costs. However, we do not expect these cases to be energetically favorable as these all correspond to the large polarons. We could partly conclude about their role on the basis of results for the same S_z-values of other $V_O^{\bullet\bullet}$ site symmetries. The energy difference ΔE_F between the most energetically favorable $S_z = 0$ for S2 case (small polaron) and the $S_z = 2$ case calculated for S4, S6 and S24 (large radius polarons) varies from 431 to 768 meV. We expect this energy difference for S2 to be in the same range. ΔE_F for $S_z = ½$ case for S2 is 301 meV and should be of similar for S6.

In our calculations with the full geometry optimization (including the lattice constants) the $V_O^{\bullet\bullet}$ formation results in monoclinic and orthorhombic lattice distortions for S2 and S4, respectively, and, consequently, separation of 4 Ce atoms into two Ce pairs. This is why three values for the changes in the Ce-Ce distances are given in Table 4 for N = 2: the change of the distances between the first pair of Ce^{3+} ions with a non-zero μ (nearest to $V_O^{\bullet\bullet}$), the distance change between the second pair of Ce^{4+} atoms with a zero μ, and lastly, the distance change between the first and second pairs of Ce atoms. For the case of S4 and N = 4 also the three values are given, representing the distance change between the Ce atoms of the first pair, second pair and between the two pairs, respectively. For the case of S6 and N = 3 two values for the Ce-Ce distances are given, i.e. the distance change between the three equivalent Ce atoms with the non-zero μ (the first value) and the distance change between one Ce atom with the zero μ and the other three atoms Ce atoms (the second value). For the case of S6 and N = 4 also two values for the distance are given, i.e. the distance change between the Ce atom with the high μ and the other

three Ce atoms with low μ, and the change of the distance between the three Ce atoms with low μ. In accordance with its low symmetry the S2 case and N = 3 is characterized by three values for the Ce-Ce distance change, viz. the two distance changes between the Ce atom with high μ and each of two Ce atoms with low μ, and the distance change between the two Ce atoms with low μ. It appears in this low symmetry case that the distances between the Ce atoms with high μ and the two Ce atoms with low μ are different. As expected the Ce atoms for the high symmetry case of S24 are not distinguishable by symmetry, and, therefore, only one value for the Ce-Ce distance is given.

As seen from table 4, the Ce-Ce distances are increased whereas the Ce-O bond lengths are decreased in all the calculated cases. In order to analyze more clearly the structural changes due to the presence of $V_O^{\bullet\bullet}$, we calculated and compared two cases with the help of the so-called 'ghost' function at the vacancy site, available in the CRYSTAL code. The 'ghost' function represents the $V_O^{\bullet\bullet}$ centered oxygen basis set and allows us to properly estimate the Ce-$V_O^{\bullet\bullet}$ bond length when the symmetry is low (Figure 3). The two cases included $S_z = 1$ of S4 (FM, small polaron) and $S_z = 2$ of S24 (FM, large polaron). As expected, the calculations with the 'ghost' functions for S4 revealed the small polaron and a zero electron charge at the vacancy site. The calculations with the ghost function for S24 evidenced the large polaron and the electron charge at the vacancy site of ~0.2 e which is most likely due to higher symmetry. Upon $V_O^{\bullet\bullet}$ formation, the two Ce^{3+} ions are displaced towards $V_O^{\bullet\bullet}$, shortening the bond length from 2.34 Å in a perfect crystal to 2.07 Å in the case of small polaron (Figure 3a). In contrast, the second pair of Ce atoms significantly increases its distance from $V_O^{\bullet\bullet}$, i.e. 2.34 to 3.04 Å.

The overall relaxation pattern is very much in a line with the fact that the volume of almost all supercells with $V_O^{\bullet\bullet}$ shown in table 4 is larger than the volume of corresponding perfect

crystal supercell (1059.19 Å^3). We found that the largest volume occurs for the small polaron solutions (~1068 Å^3). Recently, Marocchelli et al.[43,44] attributed the volume expansion effect in CeO_2 to the chemical expansion caused by increased cation size for lower oxidation states. In contast, the large polaron calculations of S24 show isotropic relaxation pattern of atoms nearest to $V_O^{\bullet\bullet}$. In fact, the effect of orbit splitting occurs also in this case. It is reflected in a separation of 24 oxygen atoms (in a perfect crystal) at distances ~ 6.6 Å from $V_O^{\bullet\bullet}$ into two groups consisting each of 12 oxygen atoms.

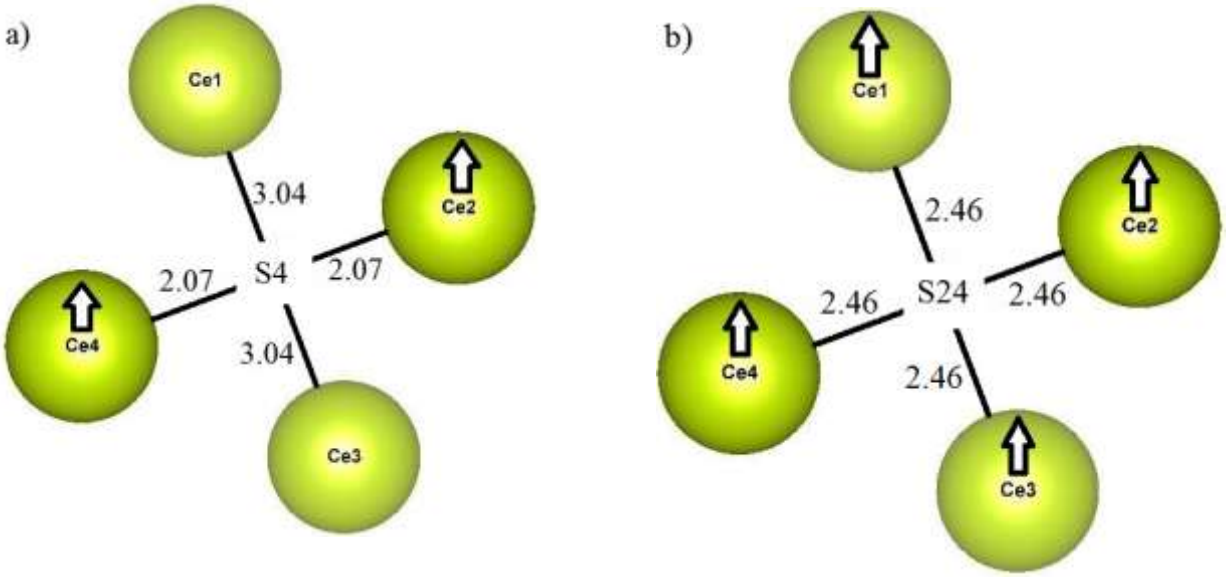

Figure 3. A schematic representation of the relaxed configuration of Ce atoms around $V_O^{\bullet\bullet}$ with (a) the spin projection $S_z = 1$ of S4 (small polaron) and (b) $S_z = 2$ of S24 (large polaron) from the calculations with the 'ghost' functions, see the text for explanations). The values represent distances in Å.

Lastly, the density of states (DOS) for two typical cases – small and large polarons – are plotted in Figure 4. As one can see, in the S2 case of small polaron Ce^{3+} *4f* levels are well

shifted (by 1.5 eV) to the low-energy side of empty Ce^{4+} 4f sub-band, whereas in the case of S6 one Ce level is close to that for the Ce^{3+} state and three other one-electron levels share another electron, having moments 0.35 μ_B each. These energy levels lie in-between the above discussed levels for Ce^{3+} and Ce^{4+}, respectively.

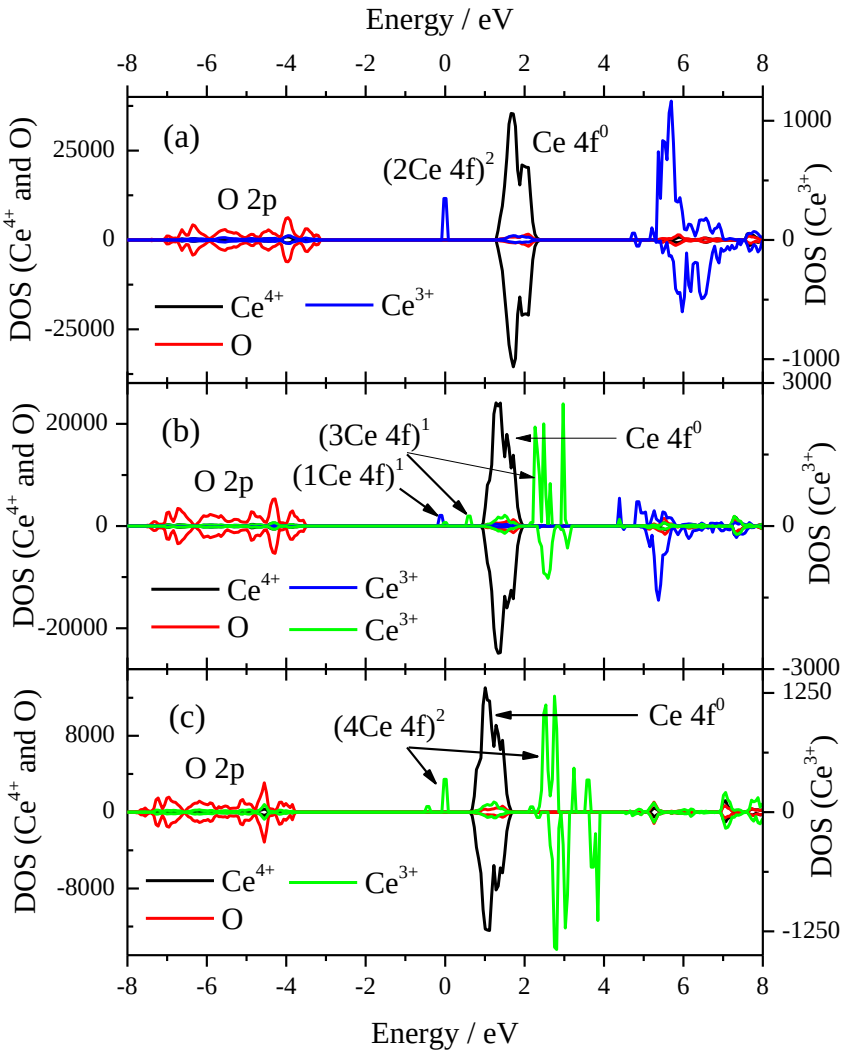

Figure 4. The partial density of states for the calculations of reduced CeO_2 with a) the spin projection $S_z = 1$ for S4 (small polaron) (b) $S_z = 2$ for S6 (large polaron), and (c) $S_z = 2$ for S24 (large radius polaron) solutions. The negative DOS values correspond to spin down electrons. All the DOS values are in arb. units. We denote those Ce atoms which have a non-zero magnetic

moment as Ce^{3+} and give their number in the parenthesis and the number localized electrons on 4f orbitals as uppercase. We denote those Ce atoms which have a zero magnetic moment as Ce^{4+} and Ce $4f^0$. The Fermi energy of α-electrons is taken as zero.

5. CONCLUSIONS

It is shown that the hybrid PBE0 (HSE06) exchange correlation functionals reproduce very well the basic properties of pure ceria. A novel approach for the defective crystals calculations in the supercell model is suggested and applied. It is based on the group-theoretical analysis of the site symmetry of the split Wyckoff positions in the perfect crystal supercell and used in the defective crystal calculations.

The novel approach mentioned shows that in CeO_2 supercell of the 3x3x3 fcc primitive cells (81 atoms) Wyckoff positions are split into 5 orbits with different site symmetries. This approach allows us to predict and obtain all possible magnetic and spatial configurations of small and large polarons in ceria.

In particular, our first principles calculations for the 3x3x3 supercell clearly demonstrate that formation of the experimentally observed small polarons occurs only when removing one oxygen atom from the 24-oxygen-atom orbit with the lowest site symmetry C_s(S2) or higher site symmetry C_{2v}(S4). The former vacancy configuration has also the lowest formation energy, which is smaller by ~0.5 eV in average than for other vacancy configurations with higher symmetry. The energy level of the polaronic state Ce^{3+} lies ~1.5 eV below the Ce-4f sub-band. The estimated small polaron migration energy of 0.6 eV is close to the experimental value[3].

The suggested approach could be applied to a wide class of defects in crystalline solids and allows the detailed analysis of electron density localization in a defective crystal and corresponding point defect formation energy.

AUTHOR INFORMATION

Corresponding Author

*E-mail: gryaznov@cfi.lu.lv. Mailing address: Institute of Solid State Physics, University of Latvia, 8 Kengaraga street, Riga, LV-1063, Latvia. Phone: +371-67187480.

ACKNOWLEDGEMENT

Authors thank R. Merkle and G. W. Watson for stimulating discussions. E. K. also acknowledges the partial financial support from the Russian Science Foundation for the study of charged defects under the project 14-43-00052. A.C. also thanks the financial support from the University of Latvia Foundation (Arnis Riekstins's "MikroTik" donation). E. K. and D. G. express their gratitude to the High Performance Computer Center in Stuttgart (HLRS, project DEFTD 12939) for the provided computer facilities whereas R.A.E. thanks St. Petersburg State University Computer Center for assistance in high-performance calculations.

REFERENCES

1. Paier, J.; Penschke, C.; Sauer, J. Oxygen Defects and Surface Chemistry of Ceria: Quantum Chemical Studies Compared to Experiment. *Chem. Rev.* **2013**, 113, 3949-3985; Steel, B.C.H.

Appraisal of $Ce_{1-y}Gd_yO_{2-y/2}$ electrolytes for IT-SOFC operation at 500 C. *Solid State Ionics*, **2000**, 129(1-4), 95-110.

2. Younis, A.; Chu, D.; Li, S. Oxygen level: the dominant of resistive switching characteristics in cerium dioxide thin films. *J. Phys. D: Appl. Phys.* **2012**, 45, 355101.

3. Naik, I. K.; Tien, T. Y. Small-polaron mobility in nonstoichiometric cerium dioxide. *J. Phys. Chem. Sol.* **1978**, 39(3), 311-315.

4. Zacherle, T.; Schriever, A.; De Souza, R. A.; Martin, M. Ab initio analysis of the defect structure of ceria. *Phys. Rev. B* **2013**, 87, 134104.

5. Castleon, C. W. M.; Lee, A. L.; Kullgren, J.; Hermansson, K. Description of polarons in ceria using Density Funational Theory. *J. Phys.: Conf. Ser.* **2014**, 526, 012002.

6. Plata, J. J.; Marquez, A. M.; Sanz, J. F. Electron Mobility via Polaron Hopping in Bulk Ceria: A First-Principles Study. *J. Phys. Chem. C* **2013**, 117, 14502-14509.

7. Keating, P. R. L.; Scanlon, D. O.; Watson, G. W. Intrinsic ferromagnetism in CeO_2: dispelling the myth of vacancy site localization mediated superexchange. *J. Phys.: Condens. Matter* **2009**, 21, 405502.

8. Ganduglia-Pirovano, M. V.; Hofmann, A.; Sauer, J. Oxygen vacancies in transition metal and rare earth oxides: Current state of understanding and remaining challenges. *Surf. Sci. Rep.* **2007**, 62, 219-270.

9. Kröger, F. A.; Vink. H. J. Relations between the Concetrations of Imperfections in Crystalline Solids. *Solid State Physics* **1956**, 3, 307-435.

10. Evarestov, R. A. Quantum Chemistry of Solids. LCAO Treatment of Crystals and Nanostructures.2nd Ed. Springer Series in Solid-State Sciences, vol. 153; Springer: Heidelberg, 2012.

11. Evarestov, R. A.; Smirnov, V. P. Supercell model of V-doped TiO_2: Unrestricted Hartree-Fock Calcualations. *Phys. Status Solidi B* **1999**, 215, 949-956.

12. Evarestov, R. A.; Smirnov, V. P. Symmetry of the Model of a Crystal with a Periodic Defect: Point Defects in MgO Crystal. *Phys. Status Solidi B* **1997**, 201 (1), 75-87.

13. Kitaev, Yu. E.; Tronc P. Ferromagnetic and antiferromagnetic ordering in the wurtzite-type diluted magnetic semiconductors. *Physics of the Solid State* 2012, 54 (3) , 490-499

14. Kroumova E., Perez-Mato, J.M. and Aroyo, M.I. *J. Appl. Cryst.* (1998) **31**, 646

15. Perdew, J. P.; Ernzerhof, M.; Burke, K. Rationale for Mixing Exact Exchange with Density Fuctional Approximations. *J. Chem. Phys.* **1996**, 105, 9982-9985.

16. Dovesi R., Saunders, V.R., Roetti, C., Orlando, R., Zicovich-Wilson, C.M., Pascale, F., Civalleri, B., Doll, K., Harrison, N.M., Bush I.J., D'Arco, Ph., Llunell, M., Causà, M., Noël, Y., *CRYSTAL14 User's Manual*; University of Turin: Turin, 2016 (http://www.crystal.unito.it/)

17. Prodan, I. D.; Scuseria, G. E.; Martin, R. L. Assessment of metageneralized gradient approximation and screened Coulomb hybrid density functionals on bulk actinides. *Phys. Rev. B* **2006**, 73, 045104.

18. Gryaznov, D.; Blokhin, E.; Sorokine, A.; Kotomin, E. A.; Evarestov, R. A.; Bussmann-Holder, A.; Maier, J. A Comparative Ab Initio Thermodynamic Study of Oxygen Vacancies in ZnO and $SrTiO_3$: Emphasis on Phonon Contribution. *J. Phys. Chem. C* **2013**, 117, 13776-13784.

19. Alkauskas, A.; Broqvist, P.; Pasquarello, A. Defect Energy Levels in Density Functional Calculations: Alignment and Band Gap Problem. *Phys. Rev. Lett.* **2008**, 101, 046405.

20. Alkauskas, A., Broqvist, P.; Devynck, F.; Pasquarello, A. Band Offsets at Semiconductor-Oxide Interfaces from Hybrid-Density Functional Calculations. *Phys. Rev. Lett.* **2008**, 101, 106802.

21. Graciani, J.; Márquez, A. M.; Plata, J.; Ortega, Y.; Hernández, N. C.; Meyer, A.; Zicovich-Wilson, C. M.; Sanz, J. F. Comparative Study on the Performance of Hybrid DFT Functionals in Highly Correlated Oxides: The Case of CeO_2 and Ce_2O_3. *J. Chem. Theory Comput.* **2011**, **7**, 56-6

22. Bredow, T.; Jug, K.; Evarestov, R. A. Electronic and Magnetic Sctructure of $ScMnO_3$. *Phys. Status Solidi* **2006**, 243, R10-R12.

23. Gryaznov, D.; Baumann, S.; Kotomin, E. A.; Merkle, R. Comparison of Permeation Measurements and Hybrid Density-Functional Calculations on Oxygen Vacancy Transport in Complex Perovskite Oxides. *J. Phys. Chem. C* **2014**, 118, 29542-29553.

24. Evarestov, R. A.; Panin, A. I.; Bandura, A. V.; Losev, M. V. Electronic Structure of Crystalline Uranium Nitrides UN, U_2N_3 and UN_2: LCAO calculations with the Basis set Optimization. *J. Phys.: Conf. Series* **2008**, 117, 012015.

25. Monkhorst J.; Pack, J. D. Special Points for Brillouin-Zone Integrations. *Phys. Rev. B* **1976**, 13, 5188-5192.

26. K. Parlinksi, Z. Q. Li, Y. Kawazoe, First-Principles Determination of Soft Mode in Cubic ZrO_2. *Phys. Rev. Lett.* **1997**, 78 (21), 4063.

27. Alfe, D. PHON: A program to calculate phonons using the small displacement method. *Comput. Phys. Commun.* **2009**, 180 (12), 2622-2633.

28. Ferrero, M.; Rérat, M.; Orlando, R.; Dovesi, R. Coupled perturbed Hartree-Fock for periodic systems: the role of symmetry and related computational aspects. *J. Chem. Phys.* **2008**, 128, 014100.

29. Ferrero, M.; Rérat, M.; Orlando, R.; Dovesi, R. The calculation of static polarizabilities in 1-3D periodic compounds. The implementation in the CRYSTAL code. *J. Comput. Chem.* **2008**, 29, 1450-1459.

30. Ferrero, M.; Rérat, M.; Kirtman, B.; Dovesi, R. Calculation of first and second static hyper-polarizabilities of 1-3D periodic compounds. Implementation in the CRYSTAL code. *J. Chem. Phys.* **2008**, 129, 244110.

31. Duclos, S.J.; Vohra, Y.K.; Ruoff, A. L; Jayaraman, A.; Espinosa, G. P.: High-pressure x-ray diffraction study of CeO_2 to 70 GPa and pressure-induced phase transformation from the fluorite structure. *Phys. Rev B* **1988**, 38, 7755.

32. Gerward, L.; Staun Olsen, J.; Petit, L.; Vaitheeswaran, G.; Kanchana, V.; Svane, A. Bulk modulus of CeO_2 and PrO_2 – An experimental and theoretical study. *J. Alloys Compounds* **2005**, 400(1-2), 56-61.

33. Wuilloud, E.; Delley, B.; Schneider, W.-D.; Baier, Y. Spectroscopic Evidence for Localized and Extended f-Symmetry States in CeO_2. *Phys. Rev. Lett*. **1984**, 53 (2), 202.

34. Nakajima, A.; Yoshihara, A.; Ishigma, M. Defect-induced Raman spectra in doped CeO_2. *Phys. Rev. B* **1994**, 50(18), 13297.

35. Voloshina, E.; Paulus, B. Influence of electronic correlations on the ground-state properties of cerium dioxide. *J. Chem. Phys.* **2006**, 124, 234711.

36. Alaydrus, M.; Sakaue, M.; Kasai, H. A DFT+U study on the contribution of 4f electrons to oxygen vacancy formation and migration in Ln-doped CeO_2. *Phys. Chem. Chem. Phys.* **2016**, 18, 12938-12946.

37. Kanoun, M. B.; Reshak, A. H.; Kanoun-Bouayed, N.; Goumri-Said S. Evidence of Coulomb correction and spin-orbit coupling in rare-earth dioxides CeO_2, PrO_2 and TbO_2: An *ab initio* study. *J. Mag. Mag. Matter.* **2012**, 324, 1397-1405

38. Kanchana, V.; Vaitheeswaran, G.; Svane, A.; Delin, A. First-principles study of elastic properties of CeO_2, ThO_2 and PoO_2. *J. Phys.: Condens. Matter* **2006**, 18(42), 9615.

39. Gürel, T.; R. Eryiğit, R. *Ab initio* pressure-dependent vibrational and dielectric properties of CeO_2. *Phys. Rev. B* **2006**, 74(1), 014302.

40. Santha, N. I.; Sebastian, M. T.; Mohanan, P.; Alford, N. Mc.; Sarma, K.; Pullar, R. C.; Kamba, S.; Pashkin, A.; Samukhina, P.; Petzelt, J. Effect of Doping on the Dielecric Properties of Cerium Dioxide in the Microwave and Far-Infrared Frequency Range. *J. Amer. Ceram. Soc.* **2004**, 87(7), 1233-1237.

41. Mochizuki, S. Infrared optical properties of cerium dioxide. *Phys. Status Solidi B* **1982**, 114(1), 189-199.

42. Wang, Yi.; Zhang, L. A.; Shang, S.; Liu, Z.-K.; Chen, L.-Q. Accurate calculations of phonon dispersion in CaF_2 and CeO_2. *Phys. Rev. B* **2013**, 88, 024304.

43. Marrocchelli, D; Bishop, S. R.; Tuller, H. L.; Yildiz, Y. Understanding Chemical Expansion in Non-Stoichiometric Oxides. Ceria and Zirconia Case Studies *Adv. Func. Mater.* **2012**, 22(9), 1958-1965.

44. Marrocchelli, D.; Bishop, S. R.; Tuller, H. L.; Watson, G. W.; Yildiz, B. Charge localization increases chemical expansion in cerium-based oxides. *Phys. Chem. Chem. Phys.* **2012**, 14, 12070-12074.

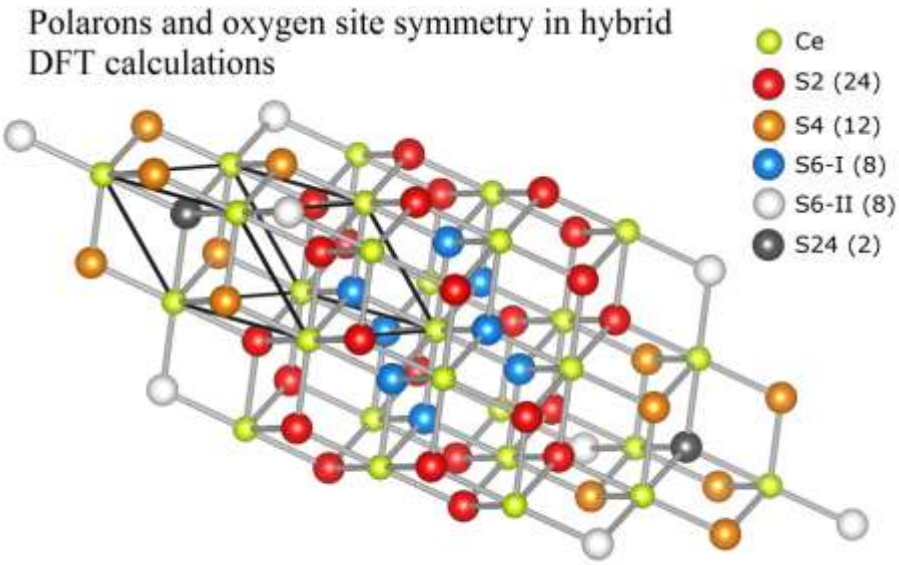

Institute of Solid State Physics, University of Latvia as the Center of Excellence has received funding from the European Union's Horizon 2020 Framework Programme H2020-WIDESPREAD-01-2016-2017-TeamingPhase2 under grant agreement No. 739508, project CAMART²